Machining characterization of polycrystalline solar material on WEDM process through response surface methodology

Raminder Singh[1a], Anish Kumar[2a*], Renu Sharma[3b]

[1]Departmentof Mechanical Engineering, M.M. Deemed to be University Mullana-Ambala-133207 (Haryana), India

[2]Departmentof Mechanical Engineering, M.M. Deemed to be University Mullana-Ambala-133207 (Haryana), India

[3]Department of Physics, M.M. Deemed to be University Mullana-Ambala-133207 (Haryana), India

[a]singh9raminder@gmail.com,[*a]anish_kaushik@rediffmail.com, [b]renuailesh@gmail.com

Abstract

The photovoltaic sector needs a high-throughput slicing method that produces minimal waste to meet rising demand. Wire electric discharge machining (WEDM) has emerged as an alternative slicing method in recent research efforts. Polycrystalline silicon is sliced using the WEDM process with a zinc-coated electrode of Ø0.25mm in diameter. Experiments were planned and conducted according to Box Behnken's design of experiments (BBDOEs). As inputs, seven different process parameters were used: PONT, PTOFF, IP, SGV, WF, WT, and WP. Response parameters measured were CS, SR, and KW. Various process parameters have also been analyzed with ANOVA methods for predictive modelling. Based on experimental data, this study determines the appropriate optimal solutions via desirability functions. During the WEDM process, the PONT, PTOFF, PC, and SV significantly influence the discharge energy on the sliced surface. As a result of this study, CS of 0.78mm^2/min, SR of 2.87µm, and KW of 0.70mm were observed by considering the parameters PONT of 119µs, PTOFF of 42µs, PC of 38A, SGV of 36V, WF of 3 mm/min, and WT of 2 kg and WP of 6 kg/cm2 at these optimal settings. Surface morphology was determined using SEM and EDX to investigate surface characteristics.

Keywords: *WEDM, Polycrystalline, Surface morphology, Box Behnken's Design (BBDOEs), Response surface methodology, Desirability*

1. Introduction

Silicon products have a wide range of applications in industry, including computers, electronics, textiles, vehicles, and architecture. The semiconductor business and its applications in electronics, microelectronics, computer systems, and the photovoltaic (PV) industry have grown rapidly in the last several decades. Hence the slicing of silicon ingots by increasing cutting speed and minimize of kerf loss is of much significance. Luque et al. [1] with a typical wafer thickness in the industry being between 250 µm and 350 µm, the kerf size was obtained with a wire saw when cutting a WC-Co composite. Muthuraman et al. [2] used a WEDM process when machining a composite material to obtain surface roughness. Luo et al. [3] employed it for the first time to cut silicon ingots in 1992. Uno et al. [4] was examined as a novel approach for

slicing mono-crystalline silicon ingots, concluding that the new method of slicing silicon ingots reduced contamination caused by wire electrode material adhesion and diffusion to the machined surface, as well as producing a lower value of surface roughness. Sreejith et al. [5] research was done on various machining methods available for silicon processing and concluded that processing of silicon wafers from silicon ingots was done as required by industrial applications using wire electric discharge machining. Peng et al. [6] wire-EDM slices medium and heavily doped silicon ingots. They were able to do this with no complications by cutting silicon wafers that were 1 mm thick without breaking the wires and using kerosene as the dielectric fluid. Takion et al. [7] experimented with wire electrical discharge machining to shape polished single crystal silicon plates and studied the results. This project's goal is to learn how to slice PV-grade silicon ingots using wire-EDM. Shah et al. [8] investigated the impact on WEDM process optimization of varying machining settings and material thicknesses in terms of material removal rate and surface roughness. The modelling strategy used led to the conclusion that the rate of material removal and the degree of surface roughness were both considerably impacted by the thickness of the work material. Yu et al. [9] looked at how adjusting the WEDM parameters might affect the machining process. An investigation into the feasibility of using wire electric discharge machining on polycrystalline silicon with a resistivity of 2-3 revealed that the open voltage was a crucial parameter for breaking the insulation of polycrystalline silicon. Singh et al. [10] studied the effects of changing the pulse on time, pulse off time, peak current, servo voltage, and wire feed on WEDM machining of AISI D2 steel. Luo et al. [11] surface potential barrier of semiconductor was shown to have a substantial influence on the cutting speed and machining parameters. Rakhwal et al. [12] investigated fabricating germanium wafers from gallium-doped ingots. The completed wafers were inspected using scanning electron microscopy and surface profilers. Singh et al. [13] dimensional precision, surface roughness, material removal rate, and scrap reduction during machining were all priorities, hence wire cut electro discharge machining was chosen as the appropriate machining method. Dongre et al. [14] wire EDM was presented as a method for slicing polycrystalline silicon that might maximize cutting speed while minimizing kerf loss and surface roughness. Joshi et al. [15] reported that wire-EDM is the best approach for slicing Si ingots with little kerf loss and a crack-free surface. Punturat et al. [16] investigated the effect of varying process settings on the sliced surface's characteristics and the degree of damage. Chuang et al. [17] studied the machining of 156mm square ingots of polycrystalline silicon and concluded that higher machining rates ($343mm^3$/min) were achieved. Murugan et al. [18] the effect of WEDM parameters on ceramic composites was studied by adjusting input factors including pulse current, on time, and off time. This observation led us to integrate experimental findings with parameters to investigate a wide variety of inputs. Verma et al. [19] material removal rate, surface roughness, and slicing speed were examined when slicing mono crystalline silicon under various conditions, including different values of open voltage, pulse on time, servo voltage, pulse off time, and wire tension. Tosun et al. [20] used a regression analysis model to look at how different machining factors affected WEDM outcomes including wire wear, crater size, and surface roughness. These parameters included pulse duration, wire speed, open circuit voltage, and dielectric cleaning pressure. The machining of silicon ingots by wire EDM is discussed in this work, and the cutting qualities are examined. This study shows that wafers can be cut from silicon ingots using WEDM by detailing the experimental setup used to make this cut. Wire cut electric discharge machining is a kind of machining that makes use of an electrical discharge to cut material (WEDM). Dielectric fluid is sent via a series of small tubes to the work area, where it fills the gap between the machined surface and the wire. Using a WEDM,

polycrystalline silicon was sliced, and the impact of various machining parameters on the rate of cutting was studied. The best parameters for cutting the materials are determined using response surface methodology. The effects of WEDM parameters such as PTON, PTOFF, PC, SGV, WF, WT, and WP were investigated.

Furthermore, past research has not explored deeply the WEDM method of cutting and surface characterization of polycrystalline material. Moreover, parametric optimization is required for better results. To analyze CS, SR, and KW in the present study, the seven parameters are taken into consideration based on past research, pilot experiments, and machine limitations as shown in **Table 2**. According to the literature, not much work has been done on the cutting of polycrystalline silicon material.

2. Material and Methods

In order to conduct this experiment, polycrystalline silicon was selected (see Table 1 material composition), and a 4-axis CNC-type WEDM (Electronica India Sprintcut, 734 Model) was used (see Figure 1). During the slicing process, CS, SR, and KW were analyzed using parameters such as pulse on time (PONT), pulse off time (PTOFF), peak current (PC), spark gap voltage (SGV), wire feed (WF), wire tension (WT), and water pressure (WP). The design matrix for the major experiment and its outputs is shown in Table 3.The Zn-coated brass wire with a diameter of Ø0.25mm was used during the WEDM process. For analysis, the sample was sliced into a square form with dimensions of (125 mm x 125 mm x 10 mm). Mitutoyo's SURFTEST was used to determine the SR of the machined surface (Model: SJ-301). Table 2 shows the factors and levels (coded and actual). An ingot of polycrystalline silicon was purchased by Tianjin Yucai Photoelectric Technology Co. Ltd. China. In conjunction with EDX, SEM (Model: JEOL, Japan, JSM-6610LV) was used to analyze surface morphology.

Table 1 Composition of polycrystalline material

Material	Chemical Composition			
Polycrystalline silicon	**C**	**Si**	**P**	**S**
	1.0%	1.31%	0.31%,	0.042%

Table 2: Parameters and their Levels (Coded and Actual)

Factors	Parameters/ Variables	Units	Actual Low Level	Actual High Level	Coded Low	Coded High
A	PONT	µs	110	125	-1	+1
B	POFFT	µs	40	55	-1	+1
C	PC	A	25	45	-1	+1
D	SGV	V	35	55	-1	+1
E	WF	mm/min	2	6	-1	+1
F	WT	kg	2	6	-1	+1
G	WP	kg/cm^2	6	10	-1	+1

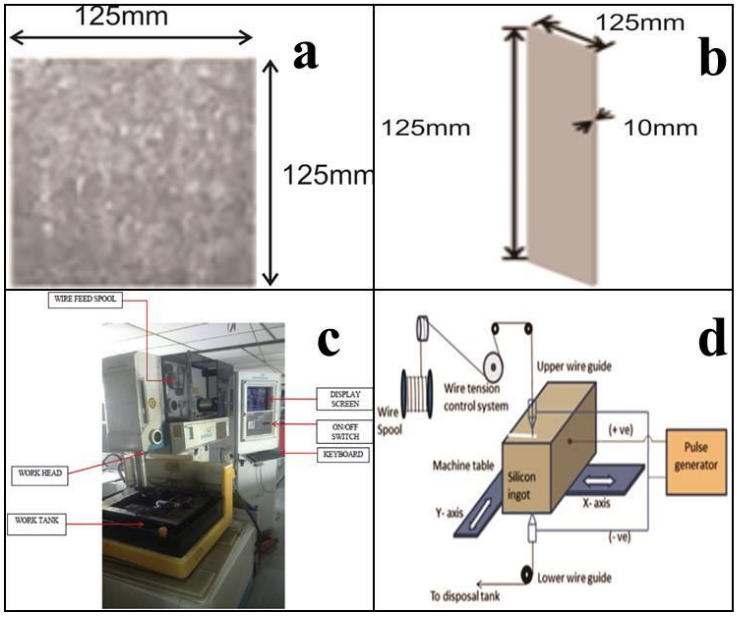

Figure 1 Slicing mechanism in WEDM Process

Table 3 Experimental Design Plan with output observations

Run	A:PONT	B:POFFT	C:PC	D:SGV	E:WF	F:WT	G:WP	CS	SR	KW
	µs	µs	A	V	mm/min	kg	kg/cm^2	mm^2/min	µm	mm
1	118	48	45	35	4	4	10	0.51	2.49	0.639
2	118	48	35	55	6	2	8	0.54	2.46	0.641
3	110	48	25	45	2	4	8	0.49	2.23	0.442
4	118	48	35	45	4	4	8	0.51	2.71	0.655
5	110	40	35	35	4	4	8	0.65	2.51	0.489
6	125	55	35	35	4	4	8	0.75	2.92	0.949
7	118	40	25	45	4	6	8	0.59	2.66	0.649
8	118	55	35	45	6	4	6	0.47	2.49	0.647
9	118	40	35	45	2	4	10	0.62	2.62	0.659
10	125	48	25	45	2	4	8	0.72	3.25	0.943
11	118	48	35	45	4	4	8	0.54	2.62	0.651
12	118	48	25	35	4	4	6	0.54	2.46	0.635
13	118	48	35	35	2	6	8	0.51	2.55	0.651
14	118	48	35	55	6	6	8	0.49	2.46	0.642
15	118	55	35	45	2	4	6	0.51	2.49	0.647

16	118	40	35	45	2	4	6	0.67	2.89	0.651
17	110	48	35	45	4	6	6	0.52	2.29	0.455
18	118	48	35	45	4	4	8	0.52	2.55	0.658
19	118	55	45	45	4	2	8	0.57	2.61	0.639
20	110	48	45	45	2	4	8	0.49	2.26	0.435
21	110	55	35	35	4	4	8	0.48	2.33	0.449
22	118	48	25	55	4	4	10	0.46	2.31	0.631
23	118	48	35	35	6	6	8	0.52	2.52	0.646
24	118	55	35	45	6	4	10	0.49	2.46	0.641
25	110	40	35	55	4	4	8	0.52	2.48	0.476
26	118	40	45	45	4	2	8	0.68	2.75	0.654
27	125	48	35	45	4	2	10	0.75	3.21	0.954
28	118	48	45	55	4	4	10	0.49	2.49	0.639
29	125	40	35	55	4	4	8	0.78	3.18	0.958
30	118	55	45	45	4	6	8	0.57	2.45	0.635
31	118	55	35	45	2	4	10	0.54	2.49	0.648
32	118	48	45	55	4	4	6	0.56	2.49	0.643
33	110	48	45	45	6	4	8	0.49	2.29	0.436
34	118	48	35	55	2	6	8	0.54	2.46	0.639
35	110	55	35	55	4	4	8	0.48	2.19	0.439
36	125	48	45	45	2	4	8	0.79	3.31	0.965
37	118	48	35	35	6	2	8	0.66	2.59	0.652
38	118	48	35	45	4	4	8	0.55	2.75	0.662
39	118	55	25	45	4	6	8	0.51	2.49	0.645
40	118	40	35	45	6	4	10	0.55	2.68	0.654
41	125	40	35	35	4	4	8	0.85	3.55	0.964
42	125	48	35	45	4	2	6	0.83	3.38	0.974
43	110	48	25	45	6	4	8	0.46	2.21	0.437
44	118	48	25	55	4	4	6	0.43	2.32	0.636
45	118	55	25	45	4	2	8	0.57	2.41	0.636

46	118	48	45	35	4	4	6	0.58	2.53	0.646
47	118	48	35	45	4	4	8	0.54	2.65	0.663
48	125	48	25	45	6	4	8	0.71	3.21	0.945
49	125	55	35	55	4	4	8	0.71	2.85	0.955
50	125	48	35	45	4	6	10	0.72	3.35	0.977
51	110	48	35	45	4	2	10	0.54	2.38	0.475
52	118	40	45	45	4	6	8	0.71	2.72	0.655
53	110	48	35	45	4	2	6	0.51	2.39	0.488
54	110	48	35	45	4	6	10	0.58	2.39	0.469
55	118	40	25	45	4	2	8	0.61	2.51	0.643
56	118	48	35	55	2	2	8	0.55	2.46	0.636
57	118	48	35	35	2	2	8	0.64	2.51	0.649
58	118	48	35	45	4	4	8	0.54	2.54	0.657
59	118	48	25	35	4	4	10	0.62	2.41	0.631
60	118	40	35	45	6	4	6	0.66	2.74	0.661
61	125	48	45	45	6	4	8	0.72	3.11	0.979
62	125	48	35	45	4	6	6	0.79	3.19	0.975

3. Measurement of responses using empirical models

3.1 Empirical modeling for responses through ANOVA

The goal of WEDM is to find optimal input variables with the least amount of noise, but this is a very challenging task. In this case, RSM can be used to evaluate the mathematical relationship between the inputs and outputs. It uses the statistical technique of Analysis of Variance to analyze the data.

3.2 Analysis of Variance and Mathematical Model for CS

ANOVA uses different test procedures to determine the significance of significant differences among the factors. Tables 4-6 present the results of ANOVA for CS, SR, and KW. By using the backward elimination rule, influential parameters are examined. Figure 2 illustrates the residual error and error deviation between predicted and actual values for CS. Furthermore, a reasonable agreement between actual and predicted values indicates that the ANOVA model meets the criteria for CS. The ANOVA for CS shows a significant F-value of 64.21. A p-value less than 0.05 indicate that the model terms are acceptable. A, B, C, D, E, F, G is an effective model term in this model, along with AF, AG, BC, BD, BG, CD, CG, and DF. With a value of 0.1412, the Lack of Fit is not significant compared to the pure error. As a result of noise, it is 64.21% likely that the F-value will be larger when the lack of fit exists. The Predicted R^2 of 0.9218 is within a feasible covenant with

the Adjusted R^2 of 0.9491, indicating that variation is below 0.2. As a result of the 34.931 S/N ratios, there is a signal that must be present in order to predict the CS.

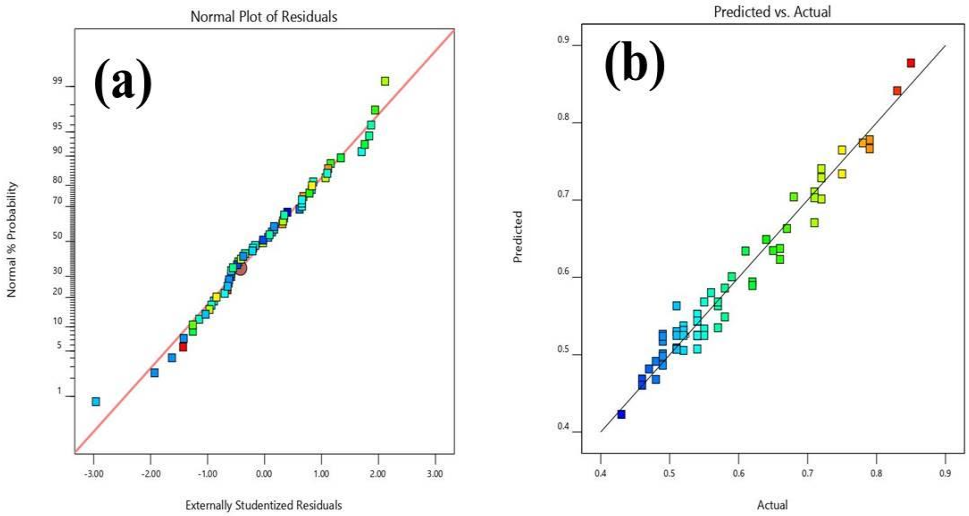

Figure 2 Graph for CS a) normal plot for residual b) predicted vs. actual

Table 4 ANOVA for CS (Reduced quadratic after backward elimination)

Source	Sum of Squares	DF	Mean Square	F-value	p-value	Remarks
Model	0.6382	18	0.0355	64.21	< 0.0001	Significant
A-PONT	0.3528	1	0.3528	638.92	< 0.0001	Significant
B-POFFT	0.0641	1	0.0641	116.01	< 0.0001	Significant
C-PC	0.0084	1	0.0084	15.28	0.0003	Significant
D-SGV	0.0241	1	0.0241	43.58	< 0.0001	Significant
E-WF	0.0040	1	0.0040	7.25	0.0101	Significant
F-WT	0.0067	1	0.0067	12.07	0.0012	Significant
G-WP	0.0017	1	0.0017	3.02	0.0895	Significant
AF	0.0018	1	0.0018	3.26	0.0780	Significant
AG	0.0072	1	0.0072	13.04	0.0008	Significant
BC	0.0021	1	0.0021	3.83	0.0570	Significant
BD	0.0032	1	0.0032	5.79	0.0204	Significant
BG	0.0055	1	0.0055	9.98	0.0029	Significant
CD	0.0066	1	0.0066	11.97	0.0012	Significant
A^2	0.1134	1	0.1134	205.40	< 0.0001	Significant
B^2	0.0222	1	0.0222	40.22	< 0.0001	Significant
F^2	0.0195	1	0.0195	35.25	< 0.0001	Significant
Lack of Fit	0.0226	38	0.0006	2.63	0.1413	not significant
					R^2	0.9641
					Adjusted R^2	0.9491
					Predicted R^2	0.9218

3.3 Analysis of Variance and Mathematical Model for SR

The quadratic model suggested by design expert software 12 is shown in Table 5 for ANOVA for SR and conformity. For surface roughness, Figure 3 shows a reasonable agreement between actual and predicted values that satisfies ANOVA's desire criteria. Backward elimination is used to eliminate parameters that fit Table 7. An F-value of 86.31 indicates that the model is significant. Noise is extremely likely to change the F-value, with a possibility of 0.01%. Therefore, 68.36% chance that a Lack of Fit F-value may happen due to noise. A, B, C, D, AB, FG, A^2, C^2, D^2 are significant model terms. Model terms with values greater than 0.1000 are not significant. When there are many insignificant model terms (excluding those required supporting hierarchy), model reduction may improve your model. Each factor contributes 71.8, 6.22, 0.68, and 0.95% respectively. The other factors have contributed very less significant to SR. As a result of coefficient estimation, the SR is expected to change with a single factor while keeping all other remaining factors constant. The Predicted R^2 of 0.9205 is close to the Adjusted R^2 of 0.9438, that is, there is a difference of less than 0.2 closer to the model. Therefore, the model is used to predict SR, taking maximum and minimum factors into account.

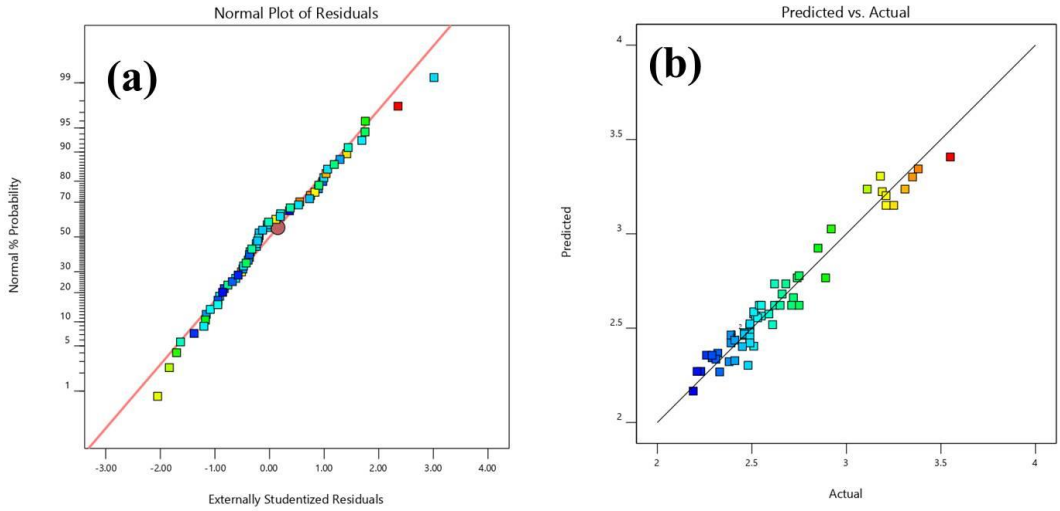

Figure 3 Graph for SR a) normal plot for residual b) predicted vs. actual

Table 5 ANOVA for SR (Reduced quadratic after backward elimination)

Source	Sum of Squares	DF	Mean Square	F-value	p-value	Remarks
Model	6.17	12	0.5146	86.31	< 0.0001	Significant
A-PONT	4.65	1	4.65	779.35	< 0.0001	Significant
B-POFFT	0.4030	1	0.4030	67.60	< 0.0001	Significant
C-PC	0.0442	1	0.0442	7.41	0.0089	Significant
D-SGV	0.0620	1	0.0620	10.40	0.0022	Significant
F-WT	0.0007	1	0.0007	0.1181	0.7326	
G-WP	0.0060	1	0.0060	1.01	0.3200	
AB	0.0300	1	0.0300	5.03	0.0294	Significant

CF	0.0221	1	0.0221	3.70	0.0603	Significant
FG	0.0242	1	0.0242	4.06	0.0494	Significant
A^2	0.6173	1	0.6173	103.55	< 0.0001	Significant
C^2	0.0792	1	0.0792	13.29	0.0006	Significant
D^2	0.1509	1	0.1509	25.31	< 0.0001	Significant
Lack of Fit	0.2566	44	0.0058	0.8206	0.6836	not significant
					R^2	0.9548
					Adjusted R^2	0.9438
					Predicted R^2	0.9205

3.4 Analysis of Variance and Mathematical Model for KW

As shown in Table 6, the ANOVA for KW and the conformity of the quadratic model was suggested by design expert software 12. Figure 4 shows are reasonable agreements between actual values and predicted values that meet the ANOVA model's desire criteria. Parameters were examined by the backward elimination rule. The model for KW, with an F-value of 2465.09, showed that the model implied significance. A 0.01% chance of noise altering the F-value is extremely high. The F-value for Lack of Fit may be 17.75% due to noise, so A, B, C, D, AB, AC, AF, FG, A^2, C^2, D^2, E^2 are significant model terms. The model terms having values are greater than 0.1000 suggested not significant. Model reduction may be useful when there are many insignificant model terms (excluding those required to support the hierarchy). PONT is responsible for 95.59% of the KW. As long as all other remaining factors remain constant, coefficient estimation describes the expected change in KW with a single factor. KW is predicted using the model with maximum and minimum factors taken into account, as shown by the Predicted R^2 of 0.9973, which is within 0.2 of the Adjusted R^2 of 0.9984.

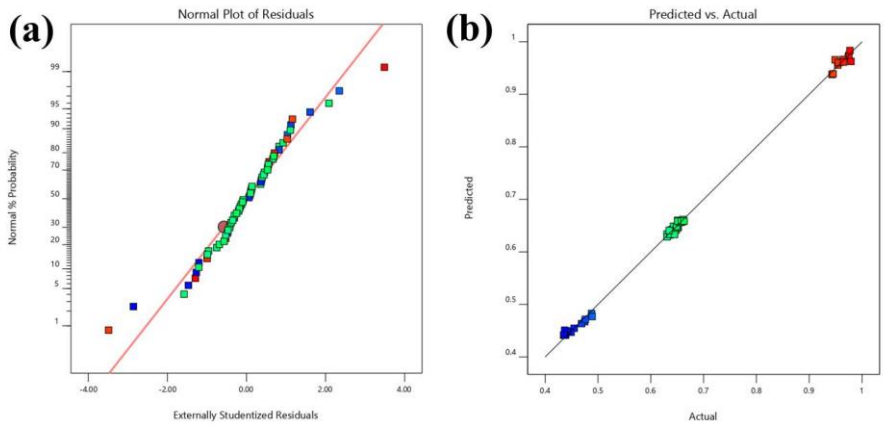

Figure 4 Graph for KW a) normal plot for residual b) predicted vs. actual

Table 6 ANOVA for KW (Reduced quadratic after backward elimination)

Source	Sum of Squares	DF	Mean Square	F-value	p-value	Remarks
Model	1.59	15	0.1060	2465.09	< 0.0001	significant
A-PONT	1.52	1	1.52	35444.17	< 0.0001	significant
B-POFFT	0.0014	1	0.0014	32.45	< 0.0001	significant
C-PC	0.0004	1	0.0004	8.20	0.0063	significant
D-SGV	0.0002	1	0.0002	4.09	0.0489	significant
E-WF	0.0000	1	0.0000	0.2481	0.6208	
F-WT	3.750E-07	1	3.750E-07	0.0087	0.9260	
G-WP	0.0001	1	0.0001	1.63	0.2083	
AB	0.0004	1	0.0004	10.12	0.0026	significant
AC	0.0005	1	0.0005	11.91	0.0012	significant
AF	0.0005	1	0.0005	11.54	0.0014	significant
FG	0.0003	1	0.0003	6.98	0.0112	significant
A^2	0.0523	1	0.0523	1217.01	< 0.0001	significant
C^2	0.0028	1	0.0028	64.03	< 0.0001	significant
D^2	0.0009	1	0.0009	20.30	< 0.0001	significant
E^2	0.0007	1	0.0007	16.89	0.0002	significant
Lack of Fit	0.0019	41	0.0000	2.31	0.1775	not significant
					R^2	0.9988
					Adjusted R^2	0.9984
					Predicted R^2	0.9973

3.5 Modeling equation for quadratic responses

For each input variable's specified value, the quadratic modelling equations established in the present study can predict the response variable. For the reduced quadratic model, the significance level =0.05 at 95CI. The following expression is a second-order quadratic polynomial regression equation for CS, SR, and KW:

CS= 21.3544 + -0.333833 x PONT + -0.0914911 x POFFT + 0.0117292 x PC + -0.0311458 x SGV + -0.00645833 x WF + -0.0232735 x WT + 0.202396 x WP + -0.001 x PONT x WT + -0.002 x PONT x WP + -0.000216667 x POFFT x PC + 0.000266667 x POFFT x SGV + 0.00175 x POFFT x WP + 0.0002875 x PC x SGV + -0.0015625 x PC x WP + 0.0013125 x SGV x WT + 0.00157447 x $PONT^2$ + 0.00069669 x $POFFT^2$ + 0.00917221 x WT^2 (1)

SR= 38.4325 + -0.752778 x PONT + 0.110667 x POFFT + 0.0666028 x PC + 0.0868435 x SGV + -0.0208333 x WT + -0.0629167 x WP + -0.00108889 x PONT x POFFT + -0.002625 x PC x WT + 0.01375 x WT x WP + 0.00367305 x $PONT^2$ + -0.00074016 x PC^2 + -0.00102141 x SGV^2 (2)

$KW = 12.7219 + -0.23121 \times PONT + -0.0164222 \times POFFT + -0.00243646 \times PC + 0.00676176 \times SGV + 0.0145863 \times WF + -0.074 \times WT + -0.00697917 \times WP + 0.000131111 \times PONT \times POFFT + 0.000106667 \times PONT \times PC + 0.000525 \times PONT \times WT + 0.00153125 \times WT \times WP + 0.00107553 \times PONT^2 + -0.000138765 \times PC^2 + -7.81399e\text{-}05 \times SGV^2 + -0.00178162 \times WF^2$ (3)

A comparative influence of factors can also be detected by equating factor coefficients. To amalgamate the dimensions of each element, the ratio is scaled. Equations 1 to 3 give the quadratic equations of the proposed model for CS, SR, and KW.

4. Results and discussion

An analysis of the responses has been demonstrated using a three-dimensional plot and a perturbation graph. Each machining parameter, along with its dielectric and parametric interactions, is analyzed in detail in the following subsection. Three-dimensional response surface graphs reveal how input variables affect response measures. In the graph, the 3D surface represents the main as well as interaction effects of two input variables at the same time, while other variables remain constant at their mid-levels. An illustration of a 3D surface's reflection is depicted by contour lines at the base of the graph. Coloured contour lines show the range of response values.

4.1 An analysis of the effect of machining parameters on CS

The research work illustrates how machine control factors have effects the CS on polycrystalline material through WEDM process. In design-Expert 12.0, the midpoint of all factors serves as a reference point. All significant parameters like A, B, C, and D have steep slopes. This indicates that CS is highly sensitive to these parameters, while E, F, and G have lower sensitivity. As a function of discharge energy, gas explosion, ion generation, and bridging effect mostly affect CS. In Table 4, we show the significant interactions between input variables such as AF, AG, BD, BG, CD, and CG. Figure 5a-f illustrates the surface plots of interactions lies at the middle point between two parameters. According to Figure 5a, CS increases sharply with an increase in PONT (A) and WP (G). Because of the higher WP (G), the debris particle is removed from the gap over a longer period due to the higher discharge energy produced by the higher PONT (A). Figures 5b and 5c also demonstrate an interaction between BD and BG effects. The effect of these interactions indicates that the CS increases from $0.515mm^2/min$ to $0.664mm^2/min$ simultaneously. Due to the constant effect of WP (G), these interactions exhibited minimal effect. Based on the interaction effect, as shown in Figure 5d-f, the CS increases from $0.546mm^2/min$ to $0.581mm^2/min$. As a result, WT (F) and WP (G) show a constant and less significant effect for CS. Due to this; a late explosion occurs and expands the spark gap in the plasma channel. Sparks are produced less often, resulting in a lower CS. This process is dependent on the weightage value of the PONT (A). As a result, low pulse settings improve production efficiency at a lower cost. The frequency of sparks is reduced when PTOFF (B) is reduced, thus reducing gas eruptions. Furthermore, higher PTOFF (B) allows sufficient time for debris to be removed from the gap zone, triggering the next batch of spark discharges.

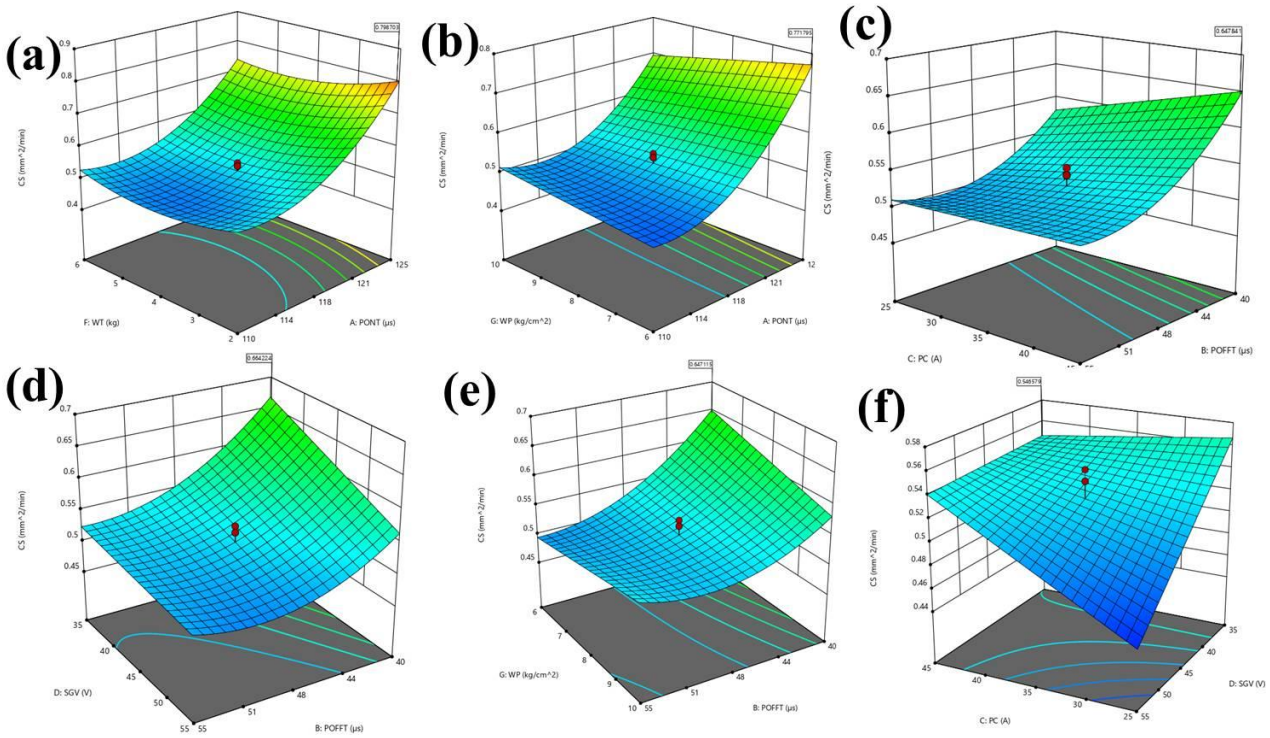

Figure 5(a-f) 3D interaction surface plots for CS

4.2. An analysis of the effect of machining parameters on SR

In Table 5, the parameters that have the greatest impact are listed. Figures 6a-c illustrates the surface plot for these parameter interactions. From Figure 6a, it can be seen that SR sharply raises (3.44µm) and then decreases (2.65µm to 2.63µm) as shown in Figures 6b-c. As a consequence, WT (F) and WP (G) show less significant effects on SR. The reason for this is that WT (F) and WP (G) have a constant and less significant effect on SR. As a result of PC, the dielectric strength decreases, and discrete sparks are avoided, and as a result of parameter B, debris from the gap zone is removed over some time. Therefore, the machining process becomes more stable, and machining performance improves. Contrary to other parameter settings, certain PTOFF (B) and PC (C) parameters have lower sensitivity. PONT and PC control the generation and discharge of ions. To achieve the best surface finish, fewer craters, voids, and micro-cracks are visible, which are mostly caused by PTOFF and PC. The significant interactions between the input variables are AB, CF, and FG, according to ANOVA Table 5.

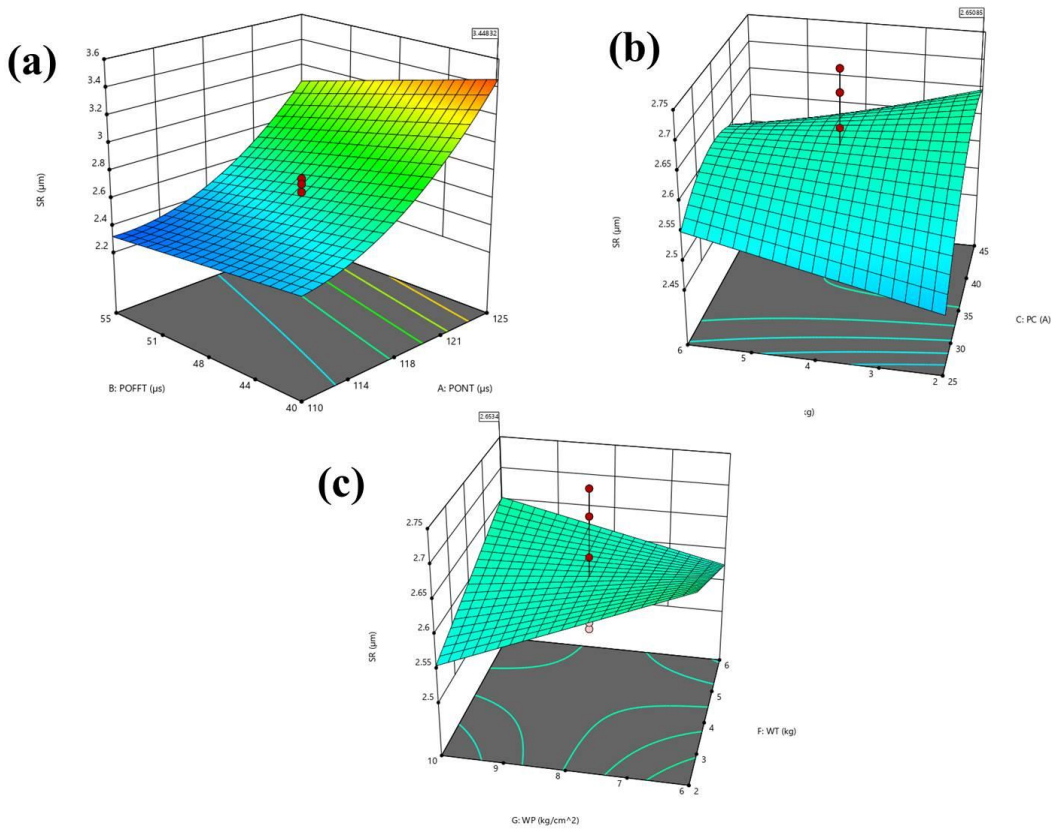

Figure 6(a-c) 3D interaction surface plots for SR

4.3 An analysis of the effect of machining parameters on KW

With changes in machining parameters, KW can increase or decrease as a result of the cutting process. As shown in Table 6, the most influential parameters are those that have the greatest impact. An analysis of the change in KW due to variation in the interaction between parameters is displayed in Figures 7a-d. Figure 7a illustrates how KW (0.967 mm) of polycrystalline material increases with concurrent decreases in POFFT (B) and increases in PONT (A). On the other hand, PONT has a significant effect on KW. By increasing PONT, more energy can be discharged for melting and vaporizing the work material. Low PTOFF values allow work material to be removed easily, while higher PTOFF values cause the substrate metal to melt when discharged intensely. Figure 7b indicates that KW is 0.967mm at higher values of PONT (125µs) and PC (45A). The amplitude of wire vibration increases when PC is high, resulting in a reduction in dielectric fluid flow around the wire, thus resulting in the inefficient removal of debris and reinforced particles from the discharge gap. In addition, the debris particles that adhered to the wire also produced high KWs. The 3D surface graph (Figure 7c) illustrates that KW increases as tension in the wire increases (0.972mm). When the wire is at a low WT, the wire amplitude is relatively high, resulting in a wider kerf. A 3D surface plot of WT and WP in Figure 7d indicates that the KW decreases (0.662mm). In Figure 7d, the effect was much less significant.

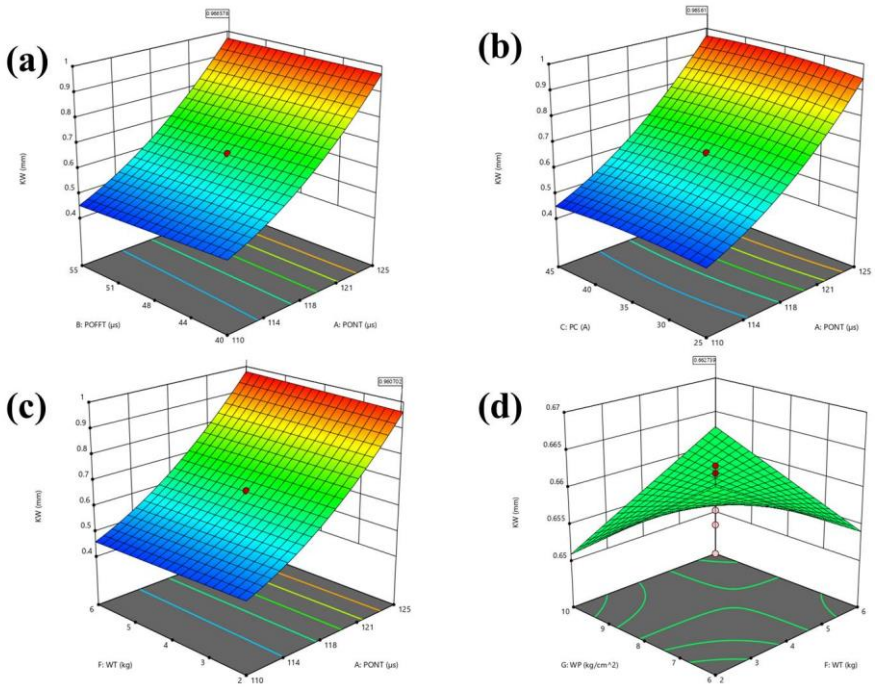

Figure 7(a-d) 3D interaction surface plots for SR

5. Surface Morphology of work material after the WEDM process

As shown in Figure 8 and 9, SEM has been used to analyze the surface morphology of machined specimens. Samples machined with Zn-coated wire exhibit micro-voids, globules, small, shallow craters, and debris particles adhered to the surface of the sample. As a result of its superior electrical conductivity, Zn-coated wire performs exceptionally well because its enlarged discharge channel prevents the melted material from re-solidifying on the work surface and makes flushing easy. The surface of the workpiece is dramatically altered during metal removal as a result of rapid heating, melting, and vaporization in the sparking zone, followed by rapid cooling. Several studies have examined the surface integrity of popular steel alloys, and composites, particularly tool and die steels, using the WEDM process. WEDM has not been adequately documented in terms of how it alters the surface properties of polycrystalline silicon. Specifically, there is not a lot of literature on polycrystalline silicon machining. Due to the uneven distribution of spherical and non-spherical agglomerates, WEDM surfaces are often rough-cut. The workpiece composition was analyzed with an energy dispersive x-ray (EDX) and metals other than the base metal were found. During WEDM, metal particles are transported from the Zn coated wire to the workpiece and the dielectric is broken down. A substantial amount of electrode material is brought to the surface of the workpiece during WEDM because not all particles can be flushed out of the spark gap. Figure 10(a-b) illustrates images of machined surfaces taken with 3KV energy dispersive X-ray (EDX). We can infer that a substantial amount of electrode material is brought to the surface of the workpiece during WEDM. Quantitative energy dispersive X-ray spectroscopy (EDX) was used to analyze the workpiece and electrodes' surface chemistry. According to EDX measurements, carbon (C), copper (Cu), oxygen (O_2), Fe, silicon (Si), and zinc (Zn) migrated to the surface of the workpiece. During machining, the Zn wire electrode melted, evaporated, and re-solidified, leaving Cu and Zn residues. The perturbation plot in Figure 11 shows four parameters, A, B, C, and D, for CS, SR, and KW of a sliced polycrystalline WEDM surface. The steep slope, which includes the most significant parameters such as A, B, and C, indicates that SR responds very strongly to these parameters.

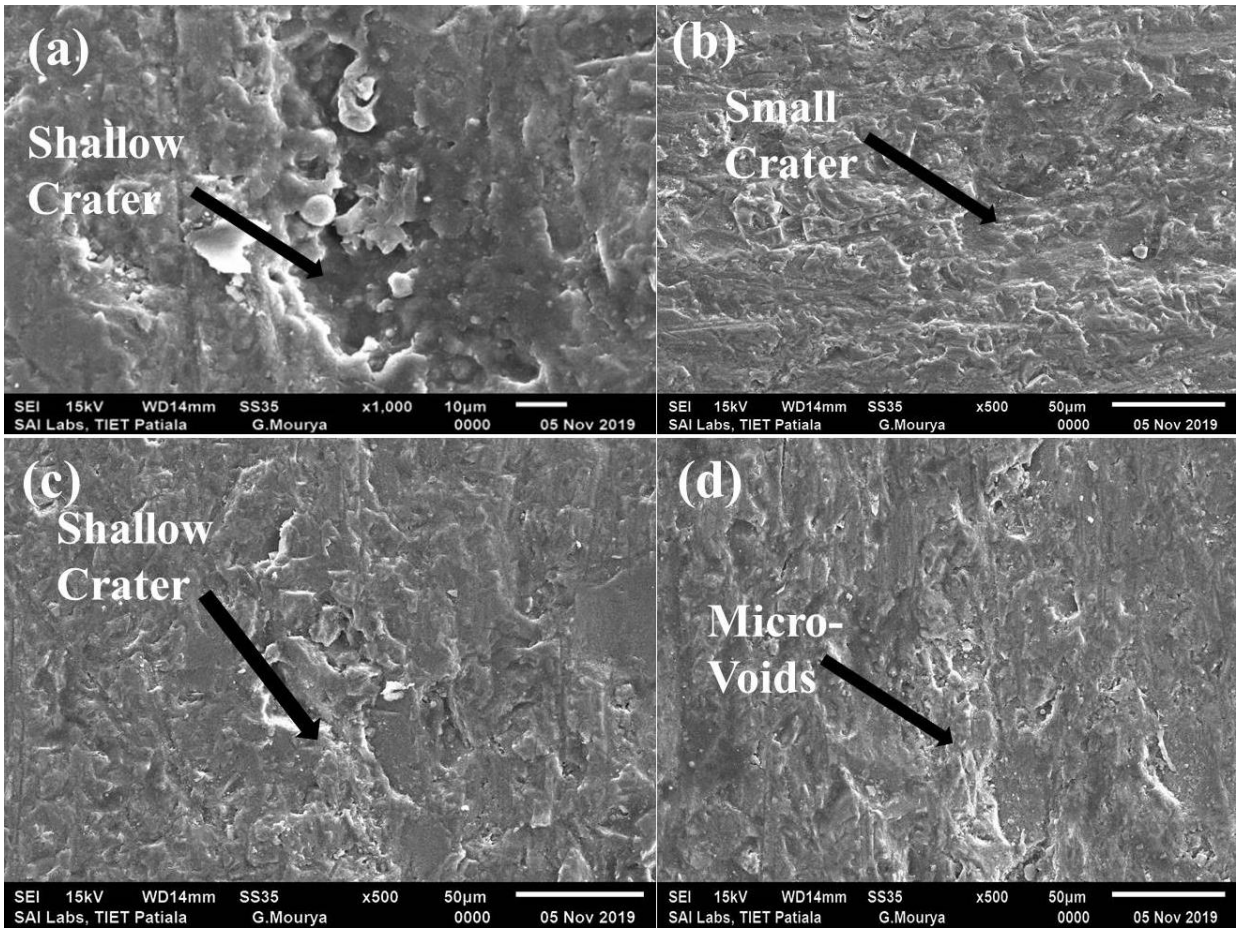

Figure 8 (Run no. 1, 35) Sub-surfaces have been appeared with wavy pattern, shallow, wider-deep craters, micro-voids

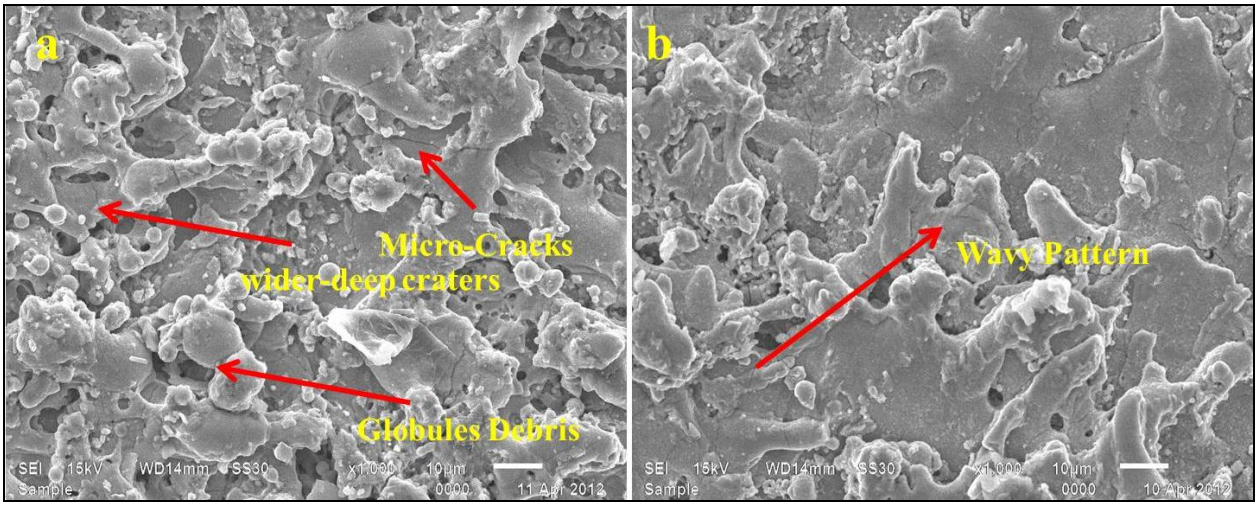

Figure 9 (Run no. 14, 25) Sub-surfaces have been appeared with wavy pattern, micro-cracks, wider-deep craters, globules of debris

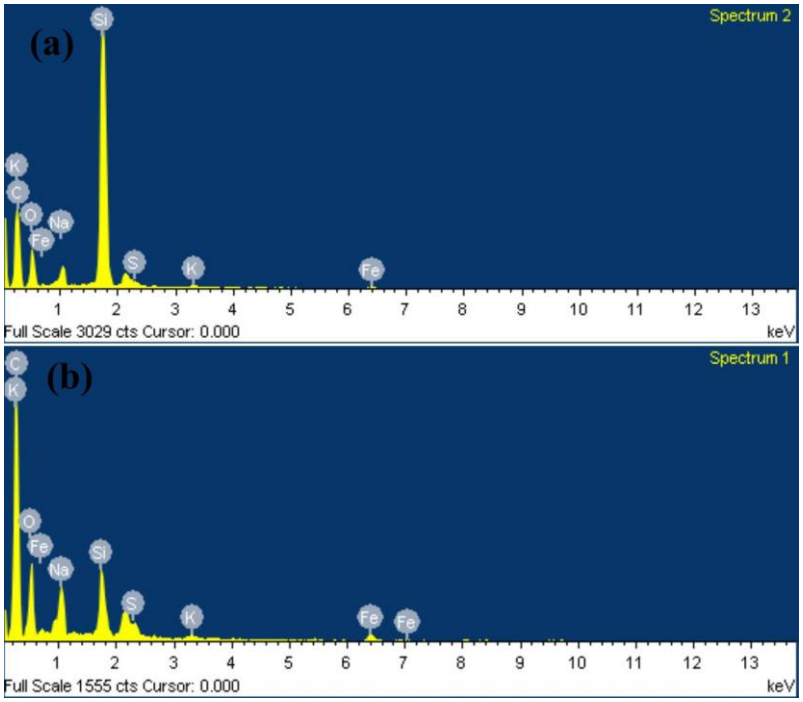

Figure 10 EDX analysis of machined samples

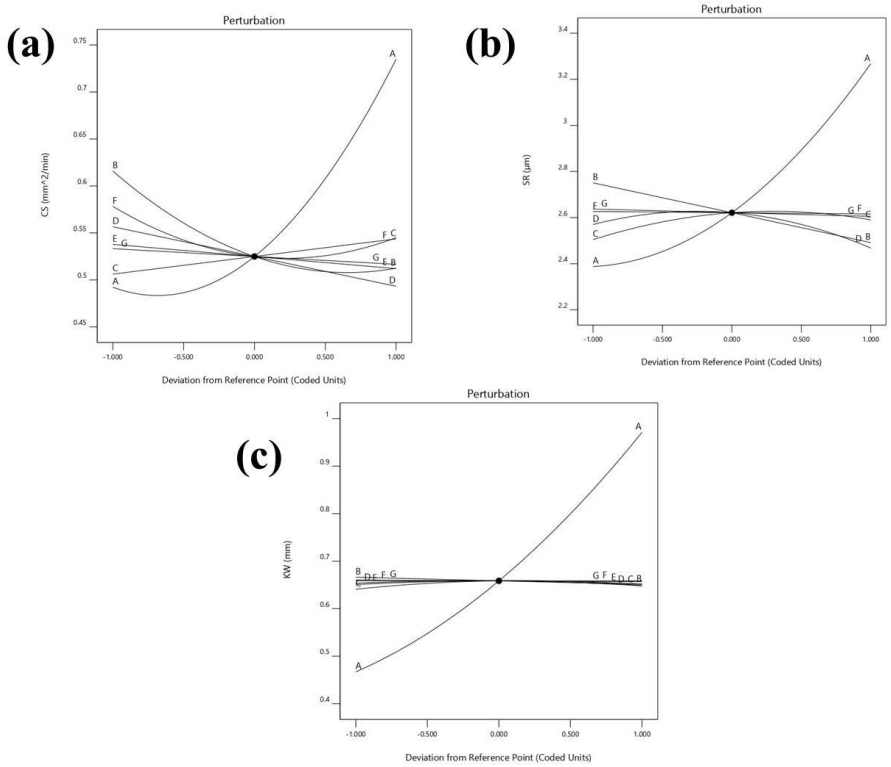

Figure 11 Perturbation plots for CS, SR and KW

6. Multi-response optimization with a desirability approach

Desirability is an objective function that increases from zero to one at the target. It is possible to transform the goal's characteristics by modifying its weight or importance. High desirability values indicate how much closer the lower and upper limits are to the best value (desirability value of 1.0) as shown in Table 7. An optimization problem with a single objective and multiple responses can be solved using the desirability approach. The desirability function for multi-responses and factors is derived from combining all goals. CS, SR, and KW are shown in Figure 12 and 13 with a ramp functions diagram and bar graph, respectively, in the numerical optimization ramps view. As a result, the point on the ramp view graph represents the estimation value for the machining parameter and response measure, making it desirable. As shown in the bar graph, the value is closer to 1, indicating satisfactory constraints. For the combined case, performance measures are considered, and their satisfactory constraint is closer to the desired value for both input and output variables.

Table 7 Optimal solution obtained through Desirability approach

S.No.	PTON	PTOFF	PC	SGV	WF	WT	WP	CS	SR	KW	Desirability
1	119	42	38	36	3	2	6	0.78	2.87	0.707	1.000
2	119	41	45	38	2	3	6	0.78	2.87	0.707	1.000
3	119	41	37	35	6	2	6	0.78	2.87	0.707	1.000
4	119	40	41	36	5	3	7	0.78	2.87	0.707	1.000
5	119	40	45	37	3	3	7	0.78	2.87	0.710	0.999
6	119	40	37	37	4	2	7	0.78	2.88	0.707	0.999
7	119	40	43	37	6	2	7	0.78	2.89	0.707	0.998
8	119	40	36	35	6	2	7	0.78	2.87	0.719	0.998
9	119	41	36	39	2	2	6	0.78	2.90	0.707	0.998
10	119	40	45	51	4	2	6	0.77	2.89	0.707	0.997
11	119	40	45	43	2	4	6	0.77	2.87	0.707	0.997
12	119	41	45	40	5	2	7	0.78	2.91	0.707	0.997
13	119	40	39	40	3	2	6	0.78	2.91	0.707	0.997
14	120	40	44	35	6	4	6	0.78	2.87	0.725	0.996
15	119	42	40	40	2	2	6	0.78	2.92	0.707	0.996
16	119	40	30	38	3	2	6	0.78	2.87	0.725	0.996
17	120	40	31	37	2	2	7	0.78	2.87	0.727	0.996
18	119	43	45	38	3	2	7	0.76	2.87	0.707	0.995
19	120	40	45	41	2	5	6	0.78	2.87	0.731	0.995
20	119	40	45	45	5	3	6	0.77	2.90	0.707	0.994

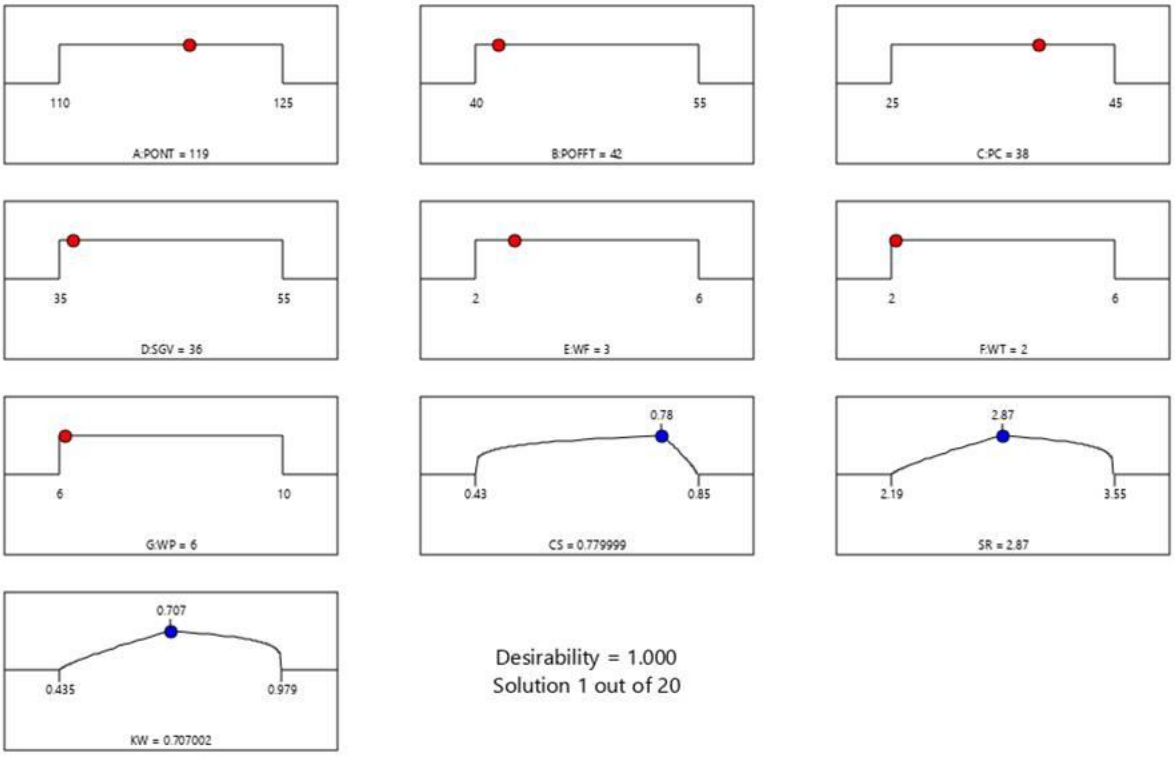

Figure 12 Ramp plot for CS, SR and KW shows the optimal solution

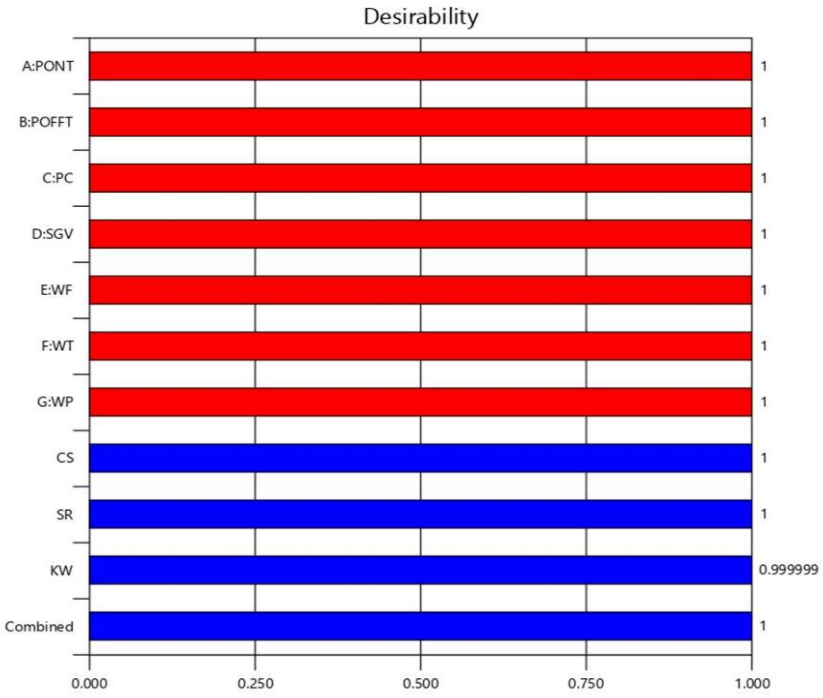

Figure 13 Bar graph for CS, SR and KW shows the combined and individual desirability

7. Conclusions

It presents an experimental and statistical analysis of wafer slicing polycrystalline silicon with WEDM at different levels of process parameters using Box Behnken's Design (BBDOEs) to measure the CS, SR, and KW. Following are the conclusions derived from the results:

1. With RSM technique, we can analyze and optimize the stochastic nature and process behavior of WEDM process.
2. Based on the results of an analysis of variance (ANOVA) of CS, SR, and KW it was found that the PONT, POFFT, PC, and SGV are the four most significant variables. In addition, a reasonable agreement between actual and predicted values indicates that the ANOVA model meets the criteria.
3. As a result, WT (F) and WP (G) show a constant and less significant effect for CS. Due to this; a late explosion occurs and expands the spark gap in the plasma channel. Sparks are produced less often, resulting in a lower CS. This process is dependent on the weightage value of the PONT (A).
4. To obtained the maximum CS (0.779mm^2/min) and minimum SR (2.87μm), KW (0.707mm) the parameters for WEDM set at PTON=119μs, PTOFF=42μs, PC=38A, SGV=36V, WT=3kg, WF= 2mm/min, and WP= 6kg/cm^2.
5. As a result of PC, the dielectric strength decreases, and discrete sparks are avoided, and as a result of parameter B, debris from the gap zone is removed over some time. Therefore, the machining process becomes more stable, and machining performance improves. Contrary to other parameter settings, certain PTOFF (B) and PC (C) parameters have lower sensitivity.
6. On the other hand, PONT has a significant effect on KW. By increasing PONT, more energy can be discharged for melting and vaporizing the work material. Low PTOFF values allow work material to be removed easily, while higher PTOFF values cause the substrate metal to melt when discharged intensely.
7. Samples machined with Zn-coated wire exhibit micro-voids, globules, small, shallow craters, and debris particles adhered to the surface of the sample. As a result of its superior electrical conductivity, Zn-coated wire performs exceptionally well because its enlarged discharge channel prevents the melted material from re-solidifying on the work surface and makes flushing easy
8. The experiment results indicated that increasing the PTON and PC values increases the kerf width of machined samples.
9. Quantitative energy dispersive X-ray spectroscopy (EDX) was used to analyze the workpiece and electrodes' surface chemistry. According to EDX measurements, carbon (C), copper (Cu), oxygen (O_2), silicon (Si), and zinc (Zn) migrated to the surface of the workpiece. During machining, the Zn wire electrode melted, evaporated, and re-solidified, leaving Cu and Zn residues.

References

1. Luque, A., Hegendus, S., 2003.Hanbook of Photovoltaic science and Engineering, Vol. 176. 1st editionWiley, New York, pp [223-225]
2. Muthuraman, V.,Ramakrishan R.,Soft modelling of Wire Electrical Discharge Machining of WC-Co composite, Advanced Materials Research Vols.335-336(2011) pp [535-540]
3. Luo, Y.F.; Chen, C.G.; Tong, Z.F. Investigation of silicon wafering by wire EDM. *Journal of Materials Science* 1992, 27 (21), [5805 – 5810]

4. Uno Y, Okada A, Okamoto Y, Hirano T. High performance slicing method of monocrystalline silicon ingot by wire EDM. In: Proceedings of the10th international conference on precision engineering (ICPE). 2001. p. [219–223].
5. Sreejith P S,: Udupa G. Recent Advances In Machining Of Silicon Wafers For Semi Conductor Applications. Int. Journal of Advanced Manufacturing Technology (2001) 17: [157-162]
6. Peng, W.Y.; Liao, Y.S. Study of electrical discharge machining technology for slicing silicon ingots. *Journal of Materials Processing Technology* 2003, 140, [274 – 279].
7. Takion, H.; Ichinohe, T.; Tanimoto, K.; Yamaguchi, S.; Nomura, K.; Kunieda, M. Cutting of polished single-crystal silicon by wire electrical discharge machining. *Precision Engineering* 2004, 28 (3), [314 – 319].
8. Shah A,; Mufti, N.; Rakwal, D.; Material removal rate, Kerf, and Surface Roughness of Tunngsten Carbide machined with Wire Electrical Discharge Machining. Journal of Materials Engineering and Performance 2010, DOI;10.1007/S11665-010-9644-y
9. Yu, PH, Lin YX,; Lee, Improvement of wire electrical discharge machining efficiency in machining Polycrystalline silicon with auxiliary pulse voltage supply. International Journal of Advanced Manufacturing Technology 2011; 57(9-12):[991-1001]
10. Singh, N.; Kumar, P.; Goyal, K. Experimental investigation of WEDM variables on surface roughness of AISI D3 die steel by using two cryogenically treated different wires. Manuf. Sci. Technol. 2014, 2, [20–25].
11. Luo, Y.F.; Chen, C.G.; Tong, Z.F. Investigation of silicon wafering by wire edm. *Journal of Materials Science* 1992, 27 (21), 5805 – 5810.
12. Rakhwal, D.; Bamberg B.,; Slicing cleaning and kerf analysis of Germanium wafers machined by wire electrical discharge machining, Journal of Material Processing Technology 209 (2009) [3740-3751]
13. H. Singh and R. Garg (2009), "Effects of Process Parameters on Material Removal Rate in WEDM", Journal of Achievements in Materials and Manufacturing Engineering, 32 (1), 70-74
14. Dongre, G.; Singh, R,; Response surface Analysis of slicing of silicon ingots with focus on Photovoltaic application, Material Science and Technology, 16 [624-652] 2012, ISSN: 1091-0344 print/1532-2483 online, DOI: 10.1080/10910344.2012.731952
15. Joshi, K.; Sharma G.,; Modeling of wire EDM slicing process for silicon, 5th International & 26th All India Manufacturing Technology, Design and Research conference (AIMTDR 2014) December 12th-14th,2014 IIT Guwahati, Assam,India
16. Punturat, J.,; Tangwarodomnukun V.,; Surface Characteristics and damage of monocrystalline silicon induced by wire-EDM, Applied Surface Science 320 (2014) [83-92]
17. Chuang, M. Mai, C,; High Efficiency Slicing of silicon ingots by Flat Wire-EDM, The 14th IFToMM World Congress,Taipei, Taiwan, October 25-30,(2015)
18. Murugan, C.,;Kumar S.; Investigations on Electric Discharge Machining Behaviour of Si_3N_4-TiN Ceramic Composite, Silicon,http//doi.org/10.1007/s12633-020-00848-w,24 November 2020
19. Verma, A.,; Singh S.,; Parametric optimization of silicon slicing using wire electro discharge machining, Materials Today Proceedings, 2214-7853/2020, Elsevier Ltd.

20. Tosun, N.,; Cogun C.,; Analysis of wire erosion and workpiece surface roughness in wire electrical discharge machining, Proc Instn Mech Engrs Vol 217 Part B: J. Engineering Manufacture

Appendix

Notation

AR^2:	Adjusted R^2
AP:	Adequate Precision
ANOVA:	Analysis of variance
BBD:	Box-Behnken Design
CI:	Confidence interval
CNC:	Computer numerical control
EDX:	Energy dispersive X-ray analysis
LOF:	Lack of fit
MS:	Mean square
PONT:	Pulse on time
POFFT:	Pulse off time
PC:	Peak current
PE:	Pure error
PR^2:	Predicted R^2
RSM:	Response surface methodology
SR:	Surface roughness
SS:	Slicing Speed
SEM:	Scanning electron microscope
SGV:	Spark gap voltage
SS:	Sum of square
WEDM:	Wire electric discharge machining
WS:	Wire speed
WT:	Wire tension